

Pituffik Titanium Project: Results of 2016 Fieldwork

Ground penetrating radar

Peter Roll Jakobsen, Ingelise Møller Balling & Samuel Weatherley



GEOLOGICAL SURVEY OF DENMARK AND GREENLAND
DANISH MINISTRY OF ENERGY, UTILITIES AND CLIMATE



Pituffik Titanium Project: Results of 2016 Fieldwork

Ground penetrating radar

Peter Roll Jakobsen, Ingelise Møller & Samuel Weatherley

1. Summary	3
2. Introduction	4
2.1 Previous onshore geophysical exploration	5
2.2 Aims.....	5
3. Survey methods	6
3.1 GPR technique	6
3.2 GPR equipment and settings	6
3.3 Positioning	8
3.4 GPR processing	9
4. Results	10
4.1 GPR lines	10
4.2 Penetration depth	11
4.3 Structures	12
4.3.1 Continuous reflection.....	12
4.3.2 Dipping reflections.....	16
4.3.3 Other reflection patterns.....	21
5. Discussion	23
5.1 The continuous reflection	23
5.2 The dipping reflections	23
5.3 Uncertainties.....	23
6. Conclusions	25
7. Recommendations	26
References	27
Appendix	
1. Map: GPR Penetration Depth	
2. Map: Location of continuous reflections	
3. Map: Occurrence of dipping reflections	
4. Table: Field notes	

1. Summary

In July and August 2016 a Ground Penetrating Radar (GPR) survey was completed on onshore raised beaches close to Moriusaq, North West Greenland (figure 1). The purpose of the investigation was to increase the baseline knowledge of titanium placer deposits that are currently being explored by FinnAust Mining Plc. Specifically, the aims of the GPR survey were to attempt to:

- map the depth to permafrost
- map the thickness of unconsolidated onshore material at Moriusaq (depth to basement)
- resolve internal structures within the material.

The survey was conducted by GEUS for FinnAust Mining.

The survey comprised 52 GPR lines with a total line length of 31.846 km. The lines were primarily measured perpendicular to the former and present shorelines in a NE-SW direction, and were connected by additional coast-parallel survey lines.

The penetration depth is between 0.5 m and 1.5 m with a mean value of 0.98 m, although 50 % of the penetration depth is between +/- 0.1 m of the mean value of 0.98 m.

A continuous reflection is observed about 1 m depth over a large part of the survey area. Typically the reflection is sub-parallel to the ground surface at c. 1 m depth, though it can be weakly undulating.

Reflections with a seaward dip are observed in a large part of the data. The reflections are most likely seaward dipping surfaces of beach ridges and/or beach planes. The beach ridge system has developed during uplift and it represents a post-glacial regression phase.

A number of other reflection patterns are observed. Some of them are related to poor penetration and lack data quality.

2. Introduction

The Thule black sand province, centred on the abandoned settlement of Moriusaq, is a region characterised by ilmenite-rich heavy mineral sands. Within this area, heavy mineral sands are distributed across active, raised and possibly also submerged beaches. This report builds on recent geological, geophysical and literature studies of the region and placer systems conducted by GEUS for Blue Jay Mining Ltd and FinnAust Mining Plc. Recent reports include a summary of the regional geology and existing data on the ilmenite potential of the region (prior to 2015) (Steensgaard et al., 2015), descriptions of geophysical offshore mapping of the seafloor and sedimentary systems conducted in 2015 (Jensen & Rödel, 2015), and a description of geological sampling activities for Blue Jay Mining in 2015 (Weatherley, 2015).

In addition to a GPR survey, field activities in the Pituffik region in 2016 for FinnAust Mining included 1) offshore geological sampling with a vibrocore (Bennike et al., 2016), 2) onshore sampling using an auger drill and by trenching (Weatherley & Johannessen, 2016), and 3) offshore profiling with a sediment echosounder (Jensen et al. 2016).



Figure 1. Location of Moriusaq, 38 km northwest of Pituffik. Blue box shows the approximate field area for 2016.

2.1 Previous onshore geophysical exploration

Previous onshore geophysical investigations of heavy mineral sands around Pituffik are restricted to magnetic and electromagnetic (EM) surveys described in Cooke (1978). Cooke (1978) took magnetic (Minimag) and EM (EM16) readings at geological sample sites. No notable magnetic or EM responses were obtained over black sand beaches. Consequently, knowledge of the thickness of the raised beach ridges and depth to the permafrost across the black sand province is limited.

2.2 Aims

The aims of the GPR survey were to

- Map the depth to the permafrost.
- If possible, to map the thickness of the beach deposits (depth to basement).
- Resolve internal structures in order to better understand the depositional environment and geological subdivisions that characterise the raised marine sediments.

3. Survey methods

3.1 GPR technique

GPR is a high-resolution geophysical technique based on the principle of high frequency electromagnetic energy propagating as waves. An electromagnetic pulse is transmitted from one antenna and the reflected signal is received at another antenna. The GPR method images structures in the ground that are related to changes in the relative dielectric permittivity (ϵ_r). The relative dielectric permittivity, ϵ_r , for geological materials encountered in this survey are air with $\epsilon_r = 1$, ice $\epsilon_r = 3-4$, fresh water $\epsilon_r = 80$, ilmenite $\epsilon_r = 54$ (Zheng et al. 2005), saturated sand $\epsilon_r = 20-30$, dry sand $\epsilon_r = 3-5$, and bedrock $\epsilon_r = 4-6$ (Davis and Annan, 1989). Small and large changes in ϵ_r give rise to reflections that are weak and strong respectively. In sediments small changes in porosity, and thereby water content, give rise to weak reflections, and beds of heavy-mineral sand can give rise to stronger reflections (Neal, 2004). In water-saturated sedimentary environments, the permafrost table generates a strong reflection (Moorman et al., 2003).

The radar wave velocity is inversely proportional to the square root of the relative dielectric permittivity in low loss materials such as sand and gravel.

A number of processes lead to damping of the radar signal. Attenuation of the electromagnetic wave is primarily controlled by the electrical conductivity of the geological materials, so a high electrical conductivity (low resistivity) causes a high attenuation of the signal. Keller (1966) reported that the resistivity of ilmenite lies in the range 10^{-3} – 4 Ohm-m. The signal can be scattered at rough interfaces or point sources, such as small ice lenses or water bubbles in the ice. At all layer boundaries with changes in ϵ_r partial reflection of the radar energy occurs. At strong reflections so much energy may be reflected that the structures beneath are masked.

3.2 GPR equipment and settings

For the GPR survey the hand towed pulseEKKO PRO system by Sensors & Software was used (Figs. 2 and 3). The GPR system was equipped with shielded 250 MHz antennas separated by a 0.38 m spacing. An odometer wheel controlled the step size, and triggered the transmitter antenna every 0.05 m. Data acquisition was controlled by a digital video logger (DVL), and the recorded data were stored on a flash-card in the DVL. The data was downloaded to a computer as well an external hard drive at the end of each working day.

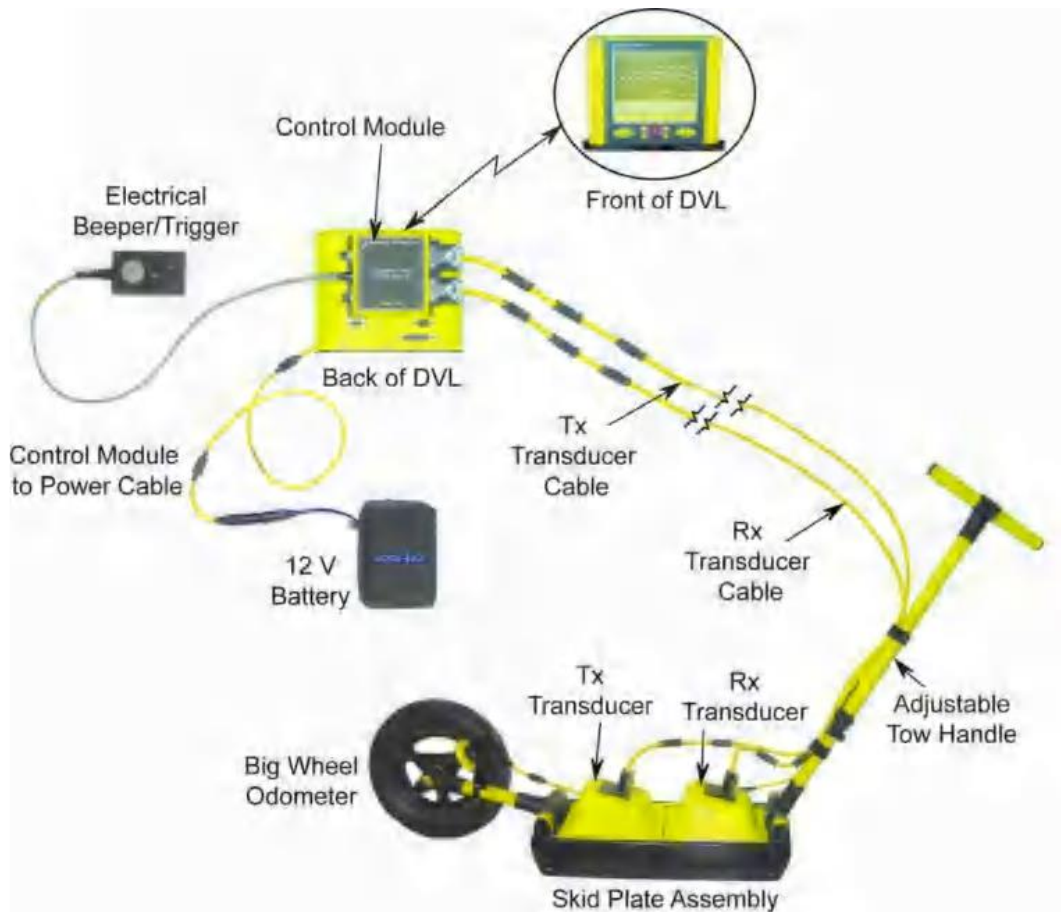


Figure 2. The complete high frequency pulse EKKO PRO tow mode assembly (Sensors & Software Inc. 2006).



Figure 3. The GPR equipment in the field. The GPS antenna was mounted on the GPR antennas and between them. The GPS unit was mounted on the GPR handle.

3.3 Positioning

For positioning a Trimble 5700 was used as a rover, and a Zephyr antenna. The antenna was mounted on the GPR antennas and the GPS unit was mounted on the GPR handle (Fig. 3).

The GPS rover data are corrected using a base mounted on one of the houses in Moriusaq (Fig. 4). The base station was established in the building containing the FinnAust crew cabin in where the generator could be kept running.

All data are recalculated to WGS84, UTM 19N and the EGM96-geoid. The position of the base station was found using the Trimble CentrePoint™ RTX™ post processing service (www.trimblertx.com<<http://www.trimblertx.com>>) with data from Julian Day 213 (31/07/2016).

The position of the base station was as follows:

Latitude: N76°45'04.61551"
Longitude: W69°50'53.56409"
Height: 25.369m (ellipsoid height)



Figure 4. *The base antenna mounted on a house in Moriusaq.*

The data for the geo radar traces were recorded online as raw GPS and simultaneously the raw observations were recorded on the rover and the base. These data were processed in Denmark and merged with the GPR data.

3.4 GPR processing

A standard editing and processing scheme is applied to the GPR data.

Firstly, all data were visually inspected to check whether the data was correctly recorded. One issue is the time-zero (time=0 at the time axis of the recorded data), which can be offset so time-zero is not the time the pulse is transmitted. Only Line 29 had a time-zero drift and was adjusted. Furthermore, the maximum penetration depth was evaluated with the purpose of reducing the time window. As the penetration depth nowhere is deeper than 60 ns the original time window was reduced to span -10 ns–90 ns.

The radar wave velocity was evaluated by inspecting diffraction hyperbolas in the GPR sections. The diffraction hyperbolas indicate velocities over a wide range from 0.06 m/ns to 0.14 m/ns. The most common velocity was approximately 0.08-0.10 m/ns. As the sediments were observed to be partly saturated with water, a radar wave velocity of 0.08 m/ns was chosen for the migration and time-to-depth conversion (Neal, 2004).

The processing steps involve (1) a “de-wow” that suppress the low-frequency inductive part of the GPR signal (Neal, 2004); (2) low-pass filtering to suppress noise at frequencies above 625 MHz; (3) an automatic gain control function (with a window width of 4 pulses) to account for geometrical spreading and attenuation; (4) migration using a constant velocity of 0.08 m/ns to properly account for reflection dip and diffractions; (5) time-to-depth conversion as well as topographic correction using a velocity of 0.08 m/ns resulting in topographically corrected GPR sections.

4. Results

4.1 GPR lines

In the period 27/07 to 7/08 2016 52 GPR lines were measured with a total length of 31.846 km (table 1). The position of each line is shown in figure 5.

line	Date	length m	orientation	line	Date	length m	orientation
2	27-jul	817.45	S-N	29	05-aug	977.55	N-S
3	27-jul	813.6	N-S	30	05-aug	961	S-N
4	27-jul	765.05	S-N	31	05-aug	946.05	N-S
5	27-jul	758.2	N-S	32	05-aug	867.65	S-N
6	29-jul	788.95	S-N	33	06-aug	435.05	N-S
7	29-jul	869.05	N-S	34	06-aug	987.4	N-S
8	29-jul	473.8	S-N	35	06-aug	134.55	NW-SE
9	30-jul	1150.25	N-S	36	06-aug	77.2	S-N
10	30-jul	1132.05	S-N	37	06-aug	76.9	N-S
11	30-jul	1118.3	N-S	38	06-aug	137.5	NW-SE
12	30-jul	1067.1	S-N	39	06-aug	171.5	NW-SE
13	30-jul	1034.2	N-S	40	06-aug	112.25	N-S
14	31-jul	930.75	S-N	41	06-aug	100	N-S
15	31-jul	869.35	N-S	42	06-aug	41.85	N-S
16	31-jul	890.75	S-N	43	06-aug	49.6	S-N
17	31-jul	444.9	N-S	44	06-aug	260.7	E-W
18	31-jul	550.95	S-N	45	06-aug	117.25	E-W
19	31-jul	1090.75	W-E	46	06-aug	88.2	E-W
20	31-jul	741.95	E-W	47	06-aug	163.05	E-W
21	01-aug	984.35	S-N	48	07-aug	166.7	W-E
23	01-aug	1018.7	N-S	49	07-aug	637.95	E-W
24	01-aug	272.05	S-N	50	07-aug	917.5	E-W
25	04-aug	1057.2	S-N	51	07-aug	353.4	S-N
26	04-aug	978.8	N-S	52	07-aug	405.9	N-S
27	05-aug	371.05	S-N	53	07-aug	463.15	E-W
28	05-aug	588.75	S-N	54	07-aug	612	W-E

Table 1. Showing the line number, date of recording, length of each line and the direction of recording. No data was collected for Line 22.

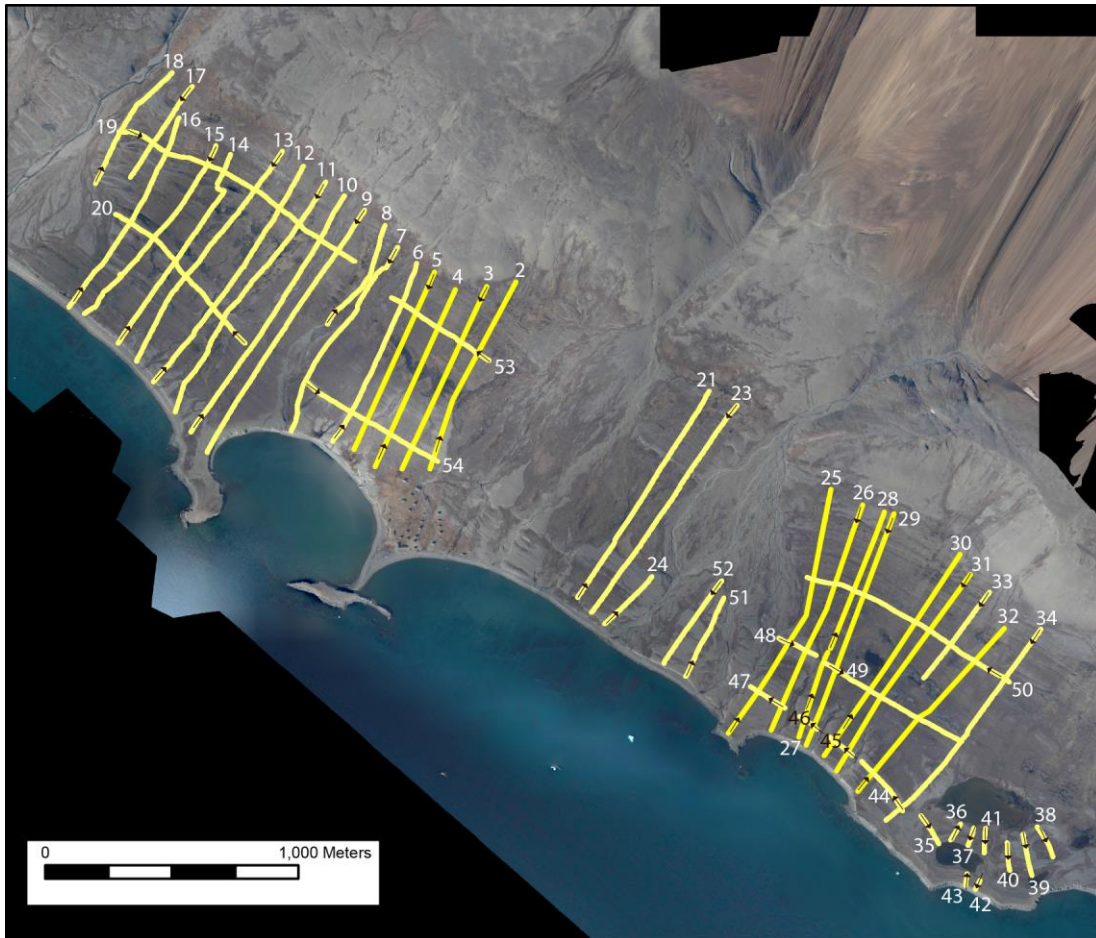


Figure 5. Position of the GPR survey lines in the Moriusaq area. Black arrows indicate the direction of travel along each line.

4.2 Penetration depth

The penetration depth is defined as the depth where the deepest reflection or reflective pattern is observed. The map in figure 6 shows the penetration depth along each of the survey lines. Any reflection patterns that are thought to relate to noise or represent multiples were excluded from the analysis presented in this section of the report.

Reflective pattern assumed to relate to noise is left out of account. This is also the case for reflection regarded as multiples.

Across the survey area, the GPR energy was often damped completely after passing a reflection at c. 1 m depth. Elsewhere the signal was gradually attenuated. The penetration depths lie between 0.5 m and 1.5 m with a mean value of 0.98 m, although 50 % of the penetration depths lie in between +/- 0.1 m of the mean value of 0.98 m.

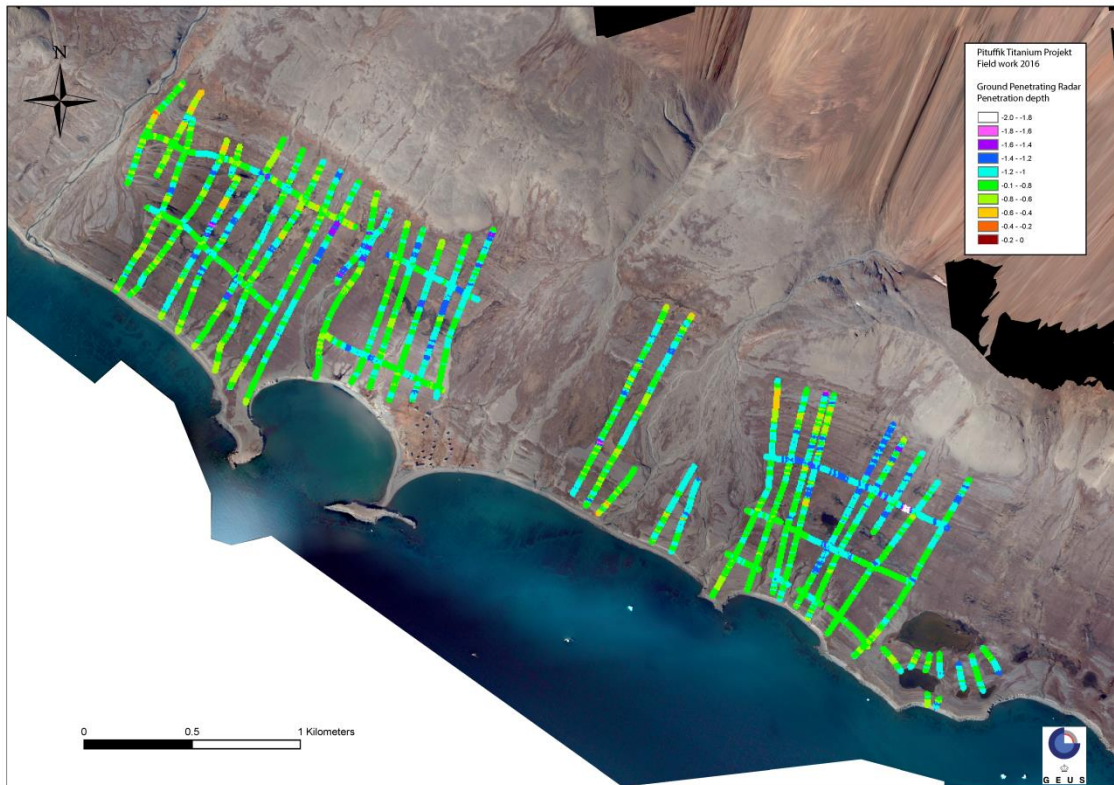


Figure 6. Map showing the penetration depth. This map is also displayed in A3 in Appendix 1.

4.3 Structures

4.3.1 Continuous reflection

A continuous reflection is present in the data at about 1 m depth in large part of the survey area. This reflection damped the GPR energy to such an extent that no reflection patterns were obtained below it. The amplitude of the reflection can be very high, moderate or weak. Typically the reflection is sub-parallel with the ground surface at c. 1 m depth, though it can be weakly undulating. Occasionally, the reflection is undulating more strongly with depth variations of c. 0.5 m within a few metres.

Figure 7 shows an example of the reflection. At position 270-300 m the reflection is weak and discontinuous. At position 300 m, the amplitude of the reflection starts to increase, and becomes very high at position 340-410 m. The reflection in Figure 7 is more or less sub-parallel to the ground surface at c. 1 m depth. Above the reflection, dipping reflections occur at 270-340 m and 340-360 m. Chaotic (340-350 m) or transparent (360-410 m) reflection patterns are present elsewhere.

At a few locations, reflections below the continuous reflection at c. 1 m are observed. In some instances these reflections are clearly identified to be multiples of the strong reflection (Figure 8, position 880-900 m). However, at other locations it is more difficult to judge

whether they are multiples or actual reflections (Figure 9, position 606-608 m, 610-612 m, 624-630 m). The occurrence and depth of the reflection is displayed in Figure 10.

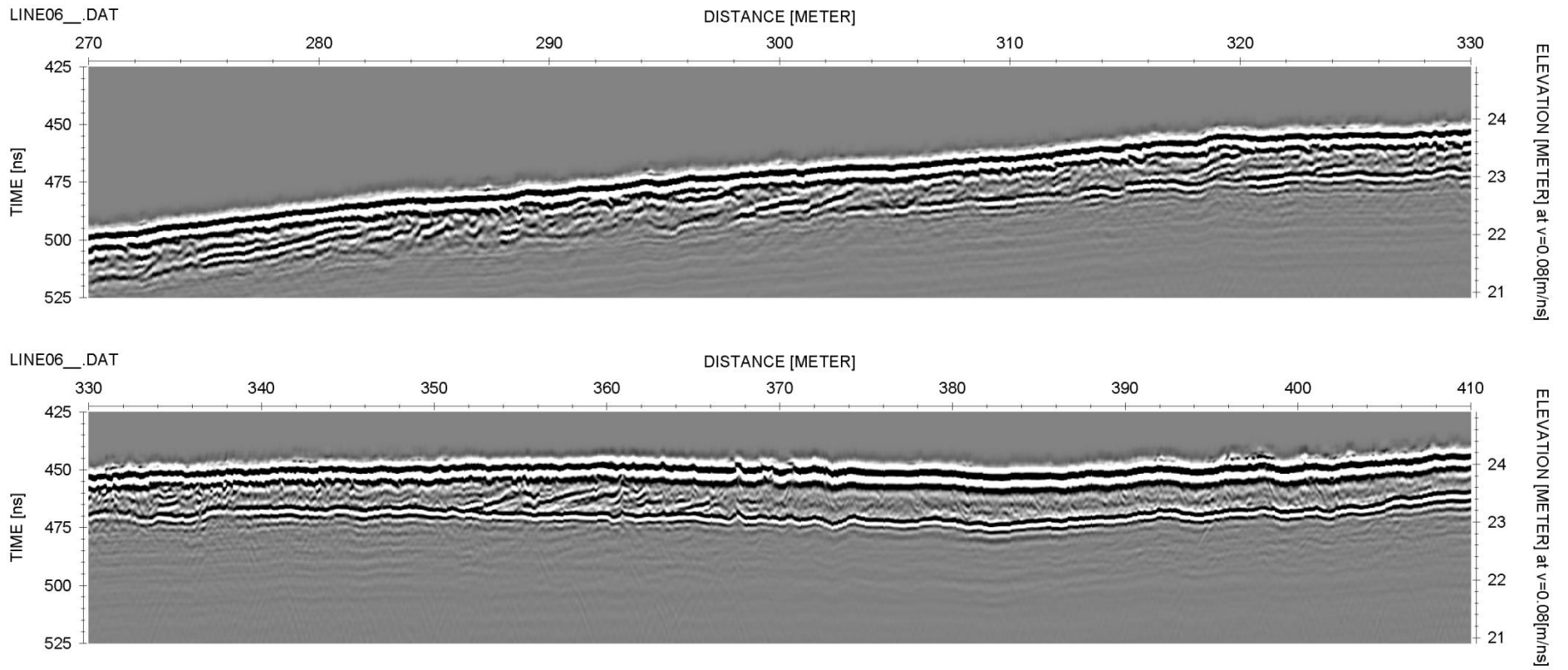


Figure 7. Example of the continuous reflection from Line 06 position 270-410 m. Vertical exaggeration x3.

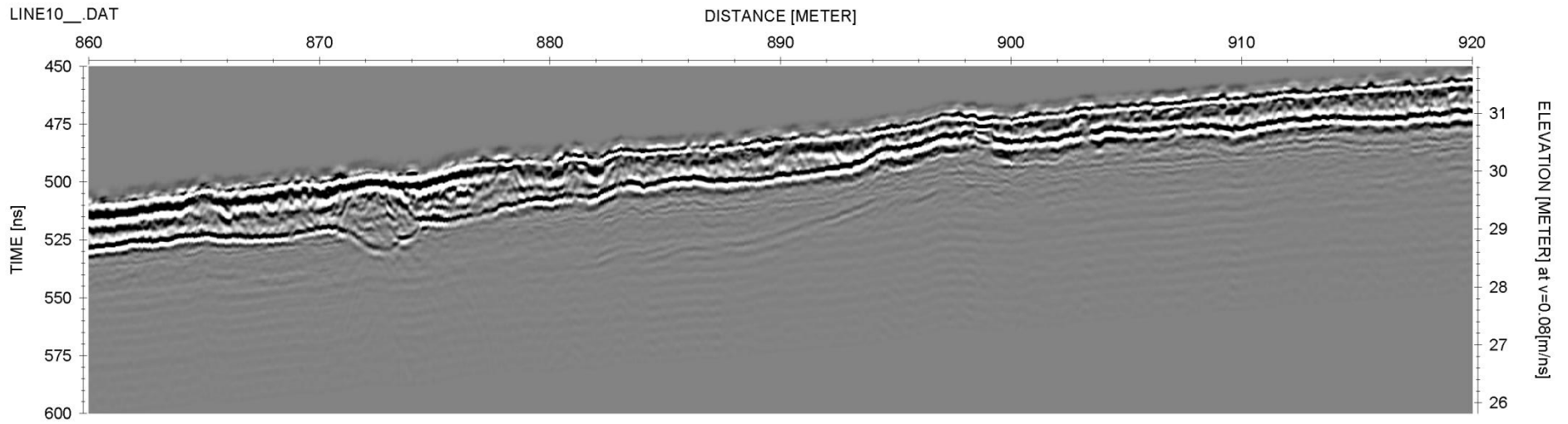


Figure 8. Example on the continuous reflection with a multiple of the reflection from Line 10, position 860-920 m. Vertical exaggeration x3.

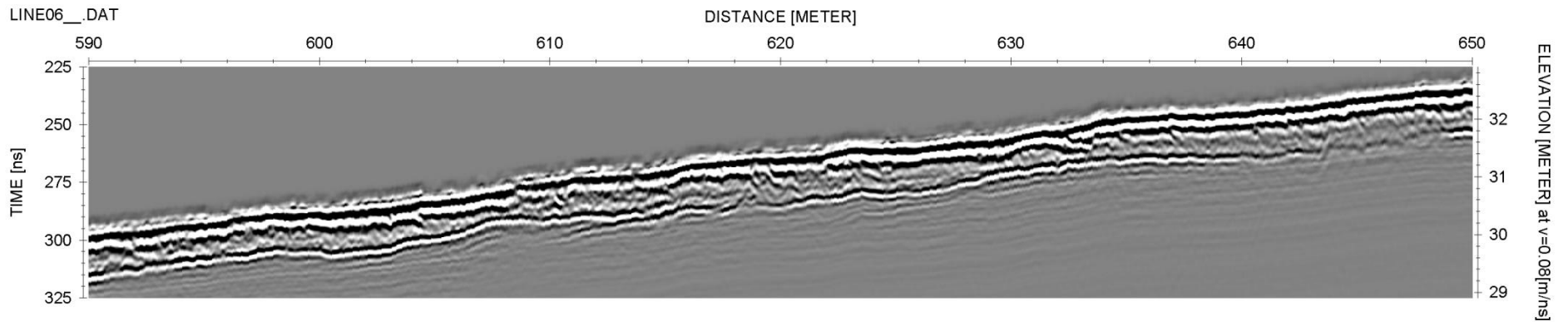


Figure 9. Example on the continuous reflection with reflections below it from Line 06, position 590-650 m. Vertical exaggeration x3.

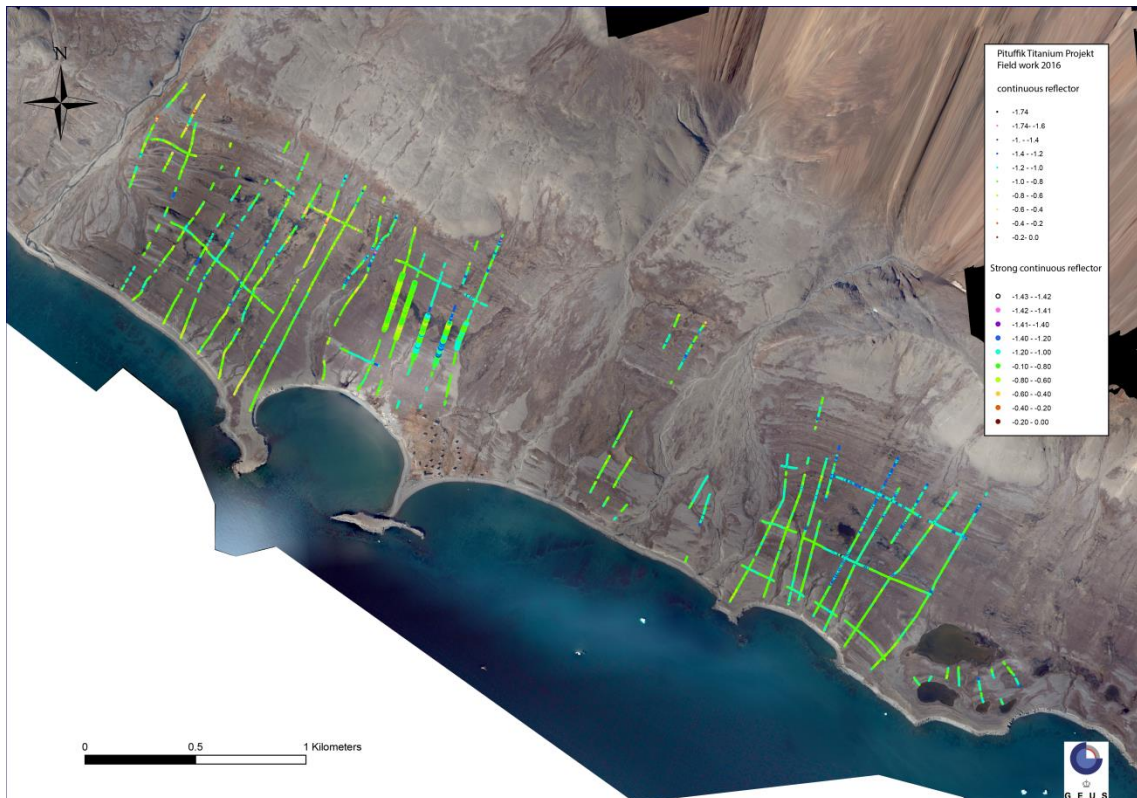


Figure 10. Map of occurrence of continuous reflections in the GPR sections. This map is also displayed in A3 in Appendix 2.

4.3.2 Dipping reflections

Reflections with a seaward dip are observed in a large part of the data. The locations of the dipping reflections in GPR sections perpendicular to the coastline are shown in Figure 11 together with sub-parallel reflections in GPR sections parallel to the coastline.

Examples of dipping reflections are shown in Figure 12-15. The occurrence of the dipping reflections varies significantly on the georadar profiles.

Some sections show very clear dipping reflections that extend from the continuous reflection at c. 1 m to the top of the GPR section (e.g. Figure 12-13). The dip of the reflections is variable. Importantly, it can be observed that less steep reflections are on-lapping with steeper dipping reflections (e.g. Figure 12, position c. 80 m).

In other sections the dipping reflections are partly attenuated and have a weak appearance just above a very weak version of the continuous reflection (e.g. Figure 14-15).

The dipping reflections appear occasionally in a more unstructured way and are irregular (Figure 14, position 290-330 m, Figure 15, position 820-850 m).

In some instances reflections appear to dip landward (e.g. Figure 15, position 860-870).

In GPR sections parallel to the coastline sets of sub-parallel reflections are observed. These sub-parallel reflections are interpreted as the perpendicular cut through the seaward dipping reflections (Figure 16).

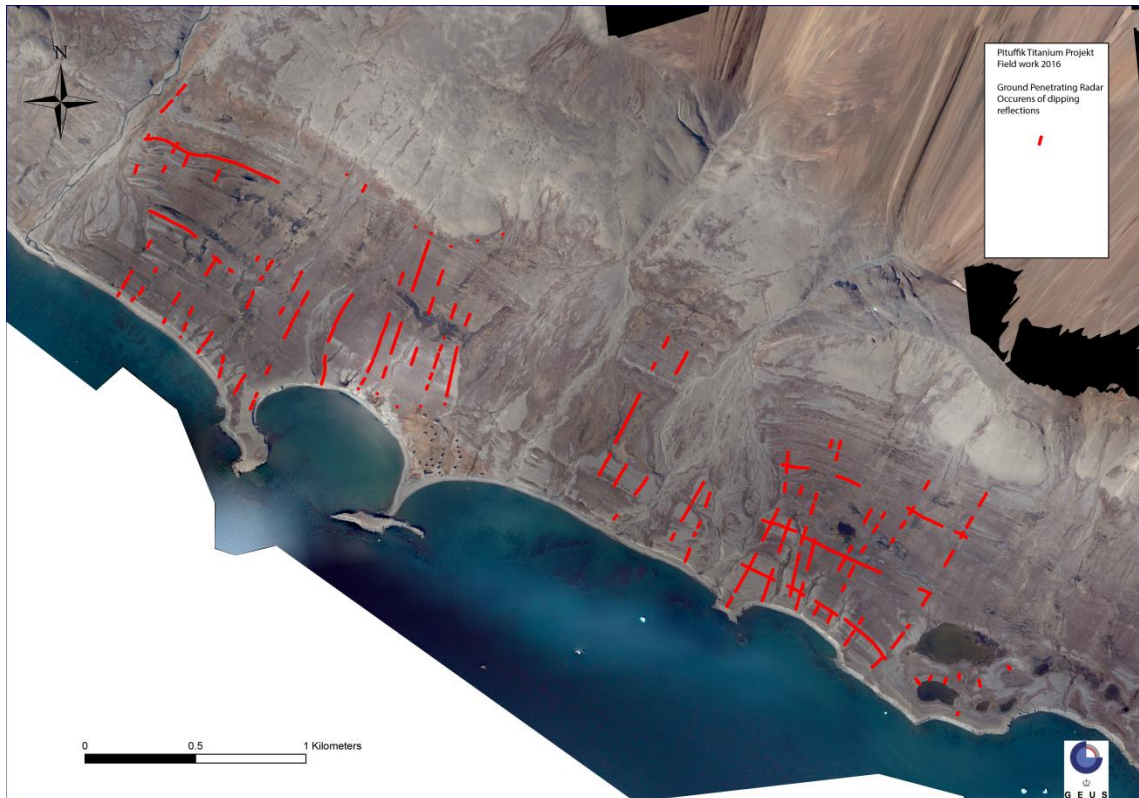


Figure 11. Map of occurrence of dipping reflections in GPR sections perpendicular to the coastline and sub-parallel reflection pattern in GPR sections parallel to the coastline. This map is also displayed in A3 in Appendix 3.

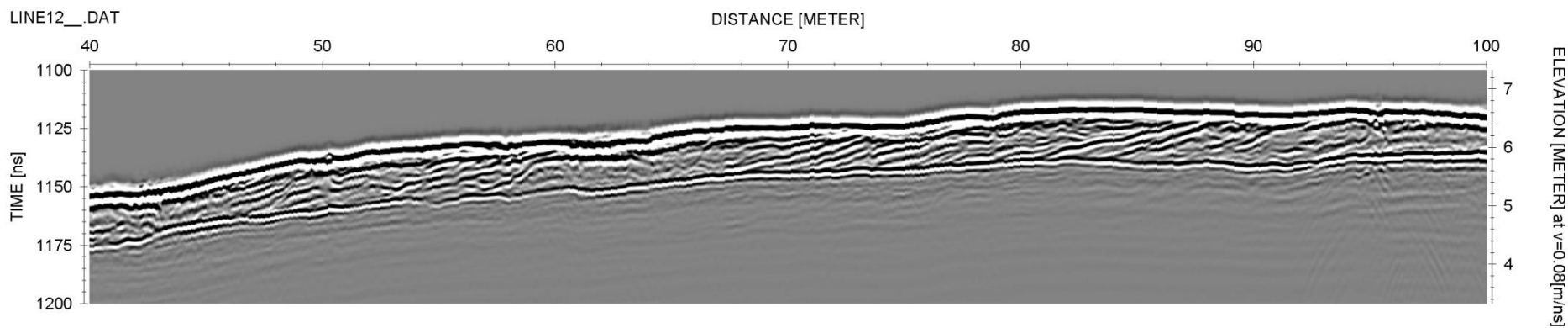


Figure 12. Example on seaward dipping reflections at Line 12, position 40-100 m. Vertical exaggeration x3.

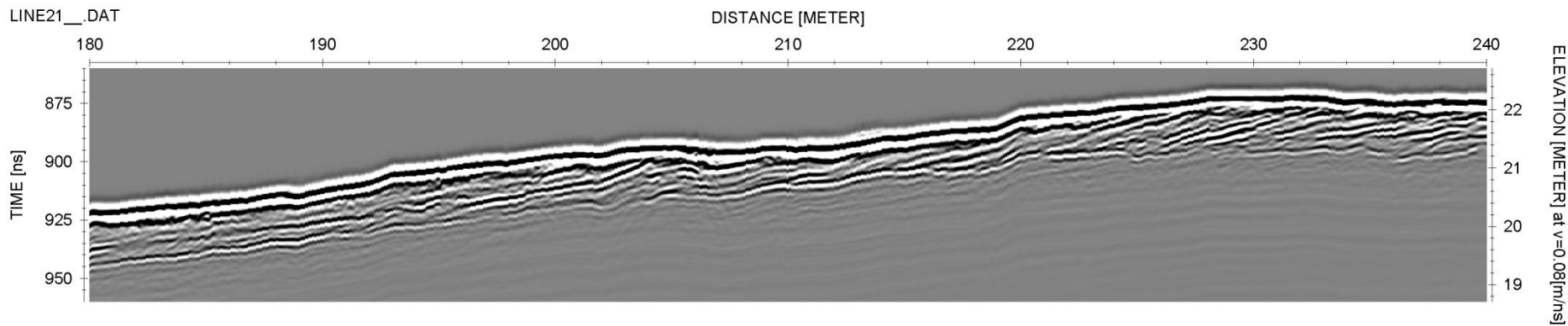


Figure 13. Example on seaward dipping reflections at Line 21, position 180-240 m. Vertical exaggeration x3.

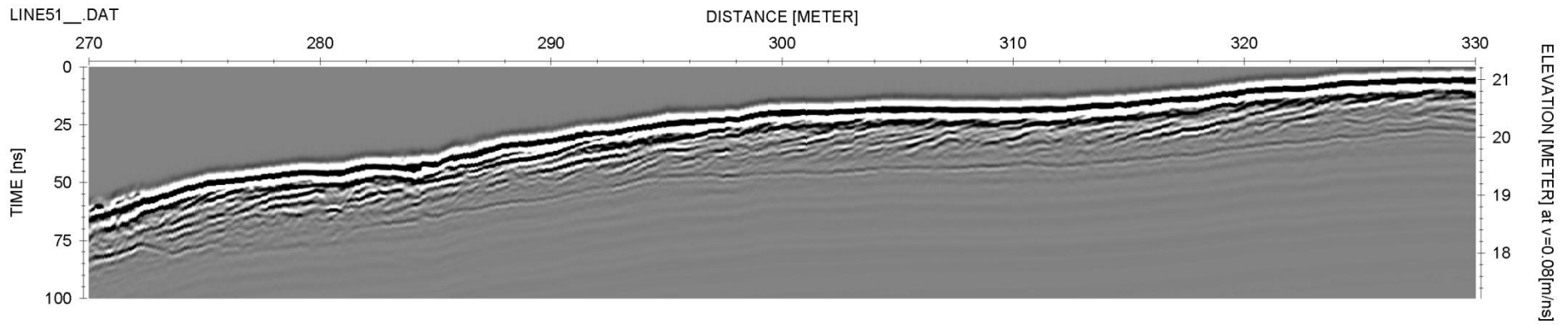


Figure 14. Example of seaward dipping reflections at Line 51, position 270-330 m. Vertical exaggregation x3.

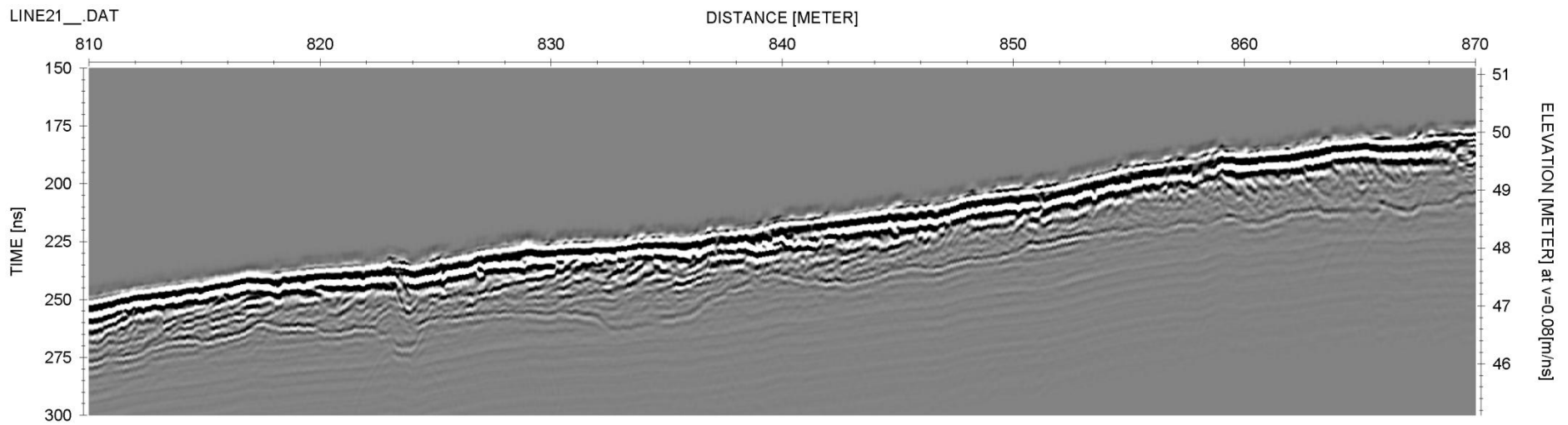


Figure 15. Example on seaward and landward dipping reflections at Line 21, position 810-890 m. Vertical exaggregation x3.

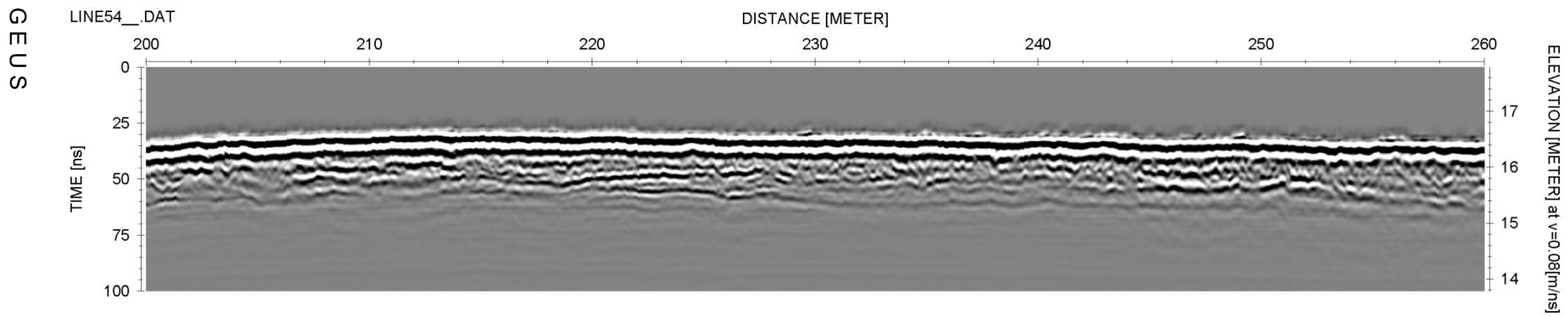


Figure 16. Example on sub-parallel, sub-horizontal reflections at Line 54, position 200-260 m. Vertical exaggeration x3.

4.3.3 Other reflection patterns

A number of other reflection patterns are observed. Some of them are associated with poor depth of penetration or poor data quality.

In Figure 17 an example is given of a GPR section showing very poor data quality and shallow penetration depth. A very high amplitude reflection close to surface or direct wave in the ground, occasionally with a rough appearance (Figure 17, position 615-630 m) limits the penetration depth significantly.

In areas where the amplitude of continuous reflection at c. 1 m is very high and the direct wave at ground surface is strong the reflection patterns in between get a transparent appearance (Figure 7, position 380-410 m).

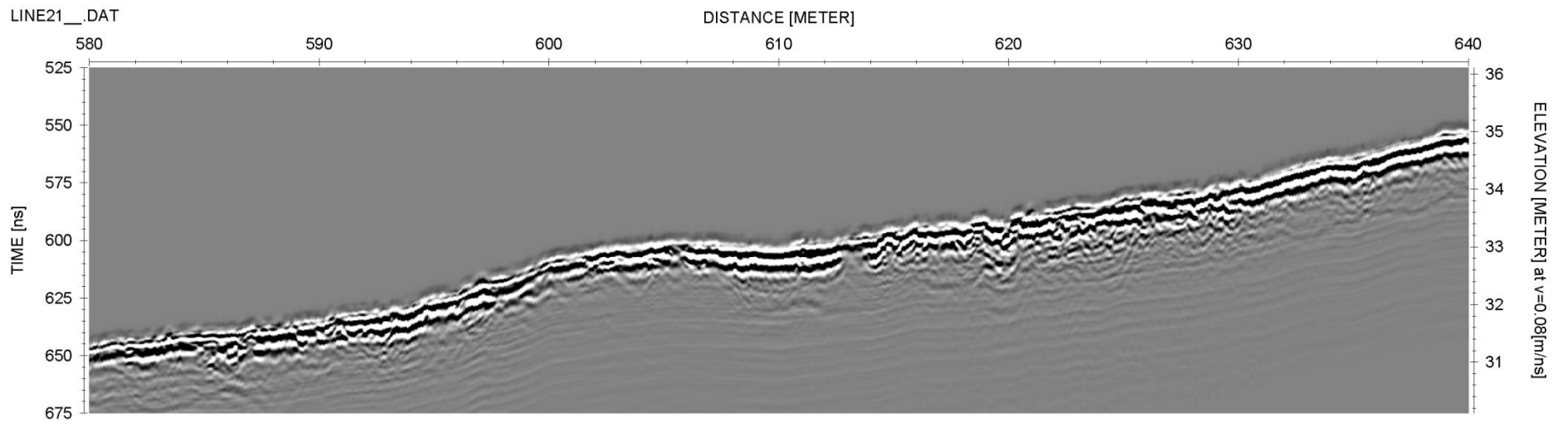


Figure 17. Example on poor data quality at Line 21, position 580-640 m. Vertical exaggeration x3.

5. Discussion

5.1 The continuous reflection

The continuous reflection observed in large parts of the survey area probably coincides with the top of the permafrost. Some trenches dug into the top metre of the sediments revealed a marked increase in the concentration of metallic minerals just above the top of the permafrost. Neal (2004) notes that thin horizons that are strongly enriched in ilmenite or other metallic minerals can generate high amplitude reflections and strongly attenuate GPR signals. This attenuating feature of metallic sands may also lead to poor signal penetration across significant parts of the survey area.

A second, although less distinct possibility, is that the continuous reflection coincides in places with the top of the bedrock. This possibility is less probable because (i) a sedimentary cap much thicker than 1 m has been observed on top of the bedrock in several places, (ii) a remarkably even top to the bedrock and sedimentary cover of consistent thickness would be required to satisfy the GPR data.

5.2 The dipping reflections

The reflections with a seaward dip are most likely seaward dipping surfaces of beach ridges and/or beach planes. They show that the beach ridge system was built up in a seawards direction. These reflections also show that the system developed during uplift and represents an overall regression phase.

5.3 Uncertainties

There are a number of uncertainties in the estimating of the depth of the continuous reflection.

The time-zero crossing can be a little imprecise and the time-zero may drift. The uncertainty is estimated to be about ± 3 ns two-way travel time, which at a radar wave velocity of 0.08 m/ns is 0.12 m.

Picking the continuous reflection can be done with an accuracy of ± 2 ns two-way travel time, which at a radar wave velocity of 0.08 m/ns is 0.08 m.

The radar wave velocity is uncertain. A constant average radar velocity of 0.08 m/ns was chosen for this study based on velocity measurements made on a number of diffraction hyperbolas. However, diffraction hyperbolas fitting other radar velocities were also observed in the GPR sections. Completely saturated sand and gravel deposits usually have radar wave velocities of 0.06 m/ns (Neal, 2004) and this radar velocity is most likely in areas where the auger holes and trenches were observed to fill with water. Other areas on the

steeper parts of the slopes are better drained and the sediments are only partly saturated and therefore the radar velocity is higher c. 0.08-0.10 m/ns. In the upper part of the GPR sections, just below the ground surface, radar velocities of c. 0.12-0.14 m/ns were occasionally are observed.

There is not enough certain velocity information in the data that a 1D or 2D velocity model can be set up; therefore a homogenous velocity model of one single velocity was used to processes the data.

The heavy mineral content in the sand would also tend to decrease the radar wave velocity (Neal, 2004).

The uncertainty of the radar wave velocity influences the calculated depth of the continuous reflection and the penetration depth. If the radar wave velocity is increased from 0.08 m/ns to 0.1 m/ns the depth is increased with 25 % (i.e. a time-to-depth converted reflection located at 1 m depth using a velocity of 0.08 m/ns would move down to 1.25 m using a velocity of 0.1 m/ns.

Comparing the reflection depth with drill-hole information would give a more precise estimate of the radar wave velocity.

6. Conclusions

The survey comprised 52 GPR lines with a total line length of 31.846 km. The lines were primarily measured perpendicular to the former and present shorelines in a NE-SW direction, and were connected by additional coast-parallel survey lines.

The penetration depth is between 0.5 m and 1.5 m with a mean value of 0.98 m. 50 % of the penetration depth is between +/- 0.1 m of the mean value of 0.98 m.

A continuous reflection is observed about 1 m depth over a large part of the survey area. Typically the reflection is oriented sub-parallel to the ground surface at c. 1 m depth, though it can be weakly undulating. The continuous reflection probably coincides with the top of the permafrost. In many places, the signal appears to disappear beneath the reflection. This is likely to be related to attenuation of the signal, and to a lesser extent, due to the strong reflection coefficient and low transmission at the permafrost boundary. An observed enrichment of ilmenite on top of the permafrost might attenuate the signal and enhance the strength of the reflection.

Reflections with a seaward dip are observed in a large part of the data. The reflections are most likely seaward dipping surfaces of beach ridges and/or beach planes. The beach ridge system has developed during uplift and it represents a post glacial regression phase.

A number of other reflection patterns are observed. Some of them are related to poor penetration and lack data quality.

7. Recommendations

Geological data from auger drilling and trenching may provide new insights to the GPR data and enable further information about the deposit to be extracted from the data. It is recommended, therefore, that the GPR data be reinterpreted alongside results from the onshore sampling programme.

It should be considered whether any other geophysical methods could be used to map the surface of the bedrock.

Future drilling programs should aim to penetrate the raised beaches to depths greater than 1 m. This would yield precise information about depth to the bedrock and confirm the nature of the strong reflection.

References

- Bennike, O., Rasmussen, M.B. & Weatherley, S. 2016. Pituffik Titanium Project: Results of 2016 Fieldwork, Offshore vibrocore sampling and core logging. GEUS Report 2016/68.
- Cook H.R. 1978: Mineral reconnaissance of the Thule district, North-WestGreenland. Rapport Grønlands Geologiske Undersøgelse **90**,17-22.
- Davis, J.L., Annan, a. P., 1989. Ground-Penetrating Radar for High-Resolution Mapping of Soil and Rock Stratigraphy. Geophys. Prospect. 531–551. doi:10.1111/j.1365-2478.1989.tb02221.x
- Jensen, J.B. & Rödel, L.G. 2015: Thule Black Sand offshore mapping. Danmarks og Grønlands Geologiske Undersøgelse Rapport 2015/74.
- Jensen, J.B., Rödel, L.G. & Weatherley, S. 2016. Pituffik Titanium Project: Results of 2016 Fieldwork, Near-shore sub-bottom profiling. GEUS Report 2016/70.
- Moorman, B.J., Robinson, S.D., Burgess, M.M., 2003. Imaging periglacial conditions with ground-penetrating radar. Permafr. Periglac. Process. 14, 319–329. doi:10.1002/ppp.463
- Neal A (2004): Ground-penetrating radar and its use in sedimentology: principles, problems and progress. - Earth-Science Reviews **66**: 261-330.
- Sensors & Software Inc. 2006: pulseEKKO users guide. Sensors & Software Mississauga, Canada.
- Steensgaard, B.M., Thrane, K., Dawes, P.R. & Bennike, O. 2015: Thule black sand province and regional geology – review and summary of data and work. Danmarks og Grønlands Geologiske Undersøgelse Rapport 2015/61, 42 pp.
- Weatherley, S. 2015: Thule Black Sands: Summary of geological sampling activities in 2015. Danmarks og Grønlands Geologiske Undersøgelse Rapport 2015/83.
- Weatherley, S. & Johannessen, P., 2016, Pituffik Titanium Project: Results of 2016 Fieldwork, Onshore sampling and sedimentology. GEUS Report 2016/69.
- Zheng, Y., Wang, S., Feng, J., Ouyang, Z., Li, X., 2005. Measurement of the complex permittivity of dry rocks and minerals: application of polythene dilution method and Lichtenecker's mixture formulae. Geophys. J. Int. 163, 1195–1202.

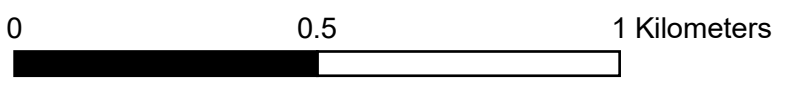
Appendix



Pituffik Titanium Projekt
Field work 2016

Appendix 1
Penetration depth, m

White	-2.0 -- -1.8
Magenta	-1.8 -- -1.6
Blue-Violet	-1.6 -- -1.4
Blue	-1.4 -- -1.2
Cyan	-1.2 -- -1
Light Green	-1 -- -0.8
Yellow-Green	-0.8 -- -0.6
Yellow	-0.6 -- -0.4
Orange	-0.4 -- -0.2
Red	-0.2 -- 0



Appendix 2

Continuous reflection
depth, m

- -1.74
- -1.74--1.6
- -1.--1.4
- -1.4--1.2
- -1.2--1.0
- -1.0--0.8
- -0.8--0.6
- -0.6--0.4
- -0.4--0.2
- -0.2--0.0

0 0.5 1 Kilometers

Pituffik Titanium Project
Fieldwork 2016
Appendix 3
Occurrence of dipping reflections



0 0.5 1 Kilometers



27-07 2016

Line 2	S-N	Time: 09.32 - 10.45
Trace no.	distance, m	Comment
0	0	Start line
98	4.05	Sample hole
1061	53	on top of broad ridge, frost polygons
5492	274.55	color change on orthophoto, backside of ridge
5742	287.05	Sample hole, water table 20 cm b.s., start of wet area
7212	360.55	start of next ridge
8120	405.95	top ridge
8534	426.65	wet area between ridges
10234	511.65	weak ridge top
12826	641.25	start of highest level
14153	707.6	ridge top in strike of sill outcrop, from here more stones
15275	763.7	start of steep rise to top level
15526	775.95	sample point just above steep rise
16350	817.45	end of line, at sample hole

Line 3	N-S	Time: 11.00 - 12.12
0	0	start highest level, some stones and boulders
811	40.5	start of sill
1202	60.05	end of sill
2109	105.4	top of ridge
2488	124.35	top of ridge
4078	203.85	start wet area
5000	249.95	top of weak ridge
7303	365.1	top of ridge between lake and stream
10520	525.95	weak ridge betweenlake and stream
16273	813.6	End of line, sample point (test hole)

Line 4	S-N	Time: 14.00 - 15.13
4279	213.9	1st low ridge on composite ridge
4682	234.05	top of 2nd ridge on composite ridge
5224	261.15	top of 3rd ridge on composite ridge
9215	460.7	top of ridge N of 'lake'
11433	571.6	top of low ridge
11955	597.7	top of low ridge
14603	730.1	top of ridge
15121	756	top of ridge more boulders from here
15302	765.05	End of line

Line 5	N-S	Time: 15.31 - 16.45
1676	83.75	weak ridge
5066	253.25	ridge
91.9	455.4	ridge
15165	758.2	End at river outlet

29/07/16

Line 6	S-N	Time: 10.40 - 12.00
2581	129.4	top ridge
6356	317.75	trench
10608	530.35	top ridge
15780	788.95	End line

Line 7	N-S	Time: 14.25 - 16.00
1946	97	change of direction, passing stream
2256	112.75	change of direction, having passed stream
5823	291.1	change of direction, passing stream
6094	304.95	change of direction, having passed stream
7420	370.95	sample no 567115
9757	488	sample no 567114
11728	586.35	sample no 567113
15457	772.8	passing stream
15611	780.5	stop passing stream
17382	869.05	end

Line 8	S-N	Time: 16.25 - 17.22
0	0	Start at river. Bedrock in riverbed
8333	416.6	start dike out-crop
9477	473.8	end

30/07/16

Line 9	N-S	Time: 9.30 - 11.30
2068	103.35	crossing water, bumpy
5036	251.75	sample no 567116 25 towards west
6283	314.1	top of ridge
6993	349.6	sample no 567117 towards west
17911	895.5	top weak ridge
21684	1084.15	trench at bay
23006	1150.35	end

Line 10	S-N	Time: 12.10 - 13.15
		continuing with 4 stacks
2053	102.6	stream
9203	460.1	top of ridge
12591	629.5	top of ridge and edge of riverbed that we have to cross
13211	660.5	other side of stream
17425	871.2	top of ridge
19389	969.4	crossing stream
21173	1058.6	in strike of sill exposed about 50 m towards west
22642	1132.05	end

Line 11	N-S	Time: 13.25 - 14.29
---------	-----	---------------------

1704	85.15	on top of sill
4417	220.8	very bumpy
5578	278.85	top of ridge
10876	543.73	top of ridge
11960	597.95	middle of stream
13529	676.4	middle of stream
16644	832.15	middle of stream
19176	958.76	sample 567126 10 m to the east
22367	1118.3	end

Line 12	S-N	Time: 15.05 - 15.55
5040	251.95	middle of stream
8647	432.3	top of ridge
21343	1067.1	end

Line 13	N-S	Time: 16.10 - 17.15
2195	109.7	top of sill
3786	189.25	top of ridge
5038	251.85	top of ridge
15255	762.7	sample 567130 about 20 m east
20685	1034.2	end at beach

31/07/16

line 14	S-N	Time: 10.00 - 11.15
198	9.85	sample 567128
1555	77.7	ridge
2421	121	sample 567129 30 m towards east
4230	211.45	top ridge
5188	259.35	top ridge
8204	410.15	top ridge
12842	642.05	top ridge
15022	751.05	top ridge, change of direction passing water
15613	780.6	change of direction
17167	858.3	top ridge
18616	930.75	end at sill out crop

Line 15	N-S	Time: 11.25 - 12.15
549	27.4	top ridge
1687	84.3	top ridge
3648	182.25	top ridge
8975	448.7	top ridge, sample 567132,
9370	468.45	top ridge
10108	505.35	top ridge
12251	612.5	top ridge
12930	646.45	top ridge
17388	869.35	end, at steep slope to recent beach

Line 16	S-N	Time: 12.55 - 13.50
2089	104.4	top ridge, sample 567135
4368	218.35	top ridge
5185	259.2	top ridge, stones
6274	313.65	top ridge, stones
7237	361.8	top ridge, gravel
7814	390.65	top ridge
8532	426.55	5 m north of top, frost wedges
9446	472.25	small ridge
10196	509.75	broad ridge
12342	617.05	top ridge
13286	664.25	top ridge
13681	684	top ridge
14784	739.2	top ridge
15439	771.9	top ridge
16904	845.15	end line, at bottom of steep slope up to upper terrasse

Line 17	N-S	Time: 14.00 - 14.30
3094	154.65	4 m down the slope
3672	183.55	bottom of slope
4149	207.4	small ridge
5574	278.65	top ridge
6126	306.25	top ridge
6714	335.65	top ridge
8090	404.45	top ridge
8899	444.9	end line at lake

Line 18	S-N	Time: 14.45 - 15.10
270	13.45	top ridge
613	30.6	top ridge
1546	77.25	top ridge
1728	86.35	top ridge
2166	105.75	top ridge
2603	130.1	top ridge
3133	156.6	top ridge
3856	192.75	top ridge
4934	246.65	possible out crop of basement
6826	341.25	start of slope
8750	437.45	on highest level
11020	550.95	end

Line 19	W-E	Time: 15.25 - 16.30
		Tie line
19691	984.5	stream
21816	1090.75	end

Line 20	E-W	Time: 17.10 - 18.15
9024	451.15	Middle of broad stream, steep sides

11256 562.75 Sample 567132
 14840 741.95 end

01/08/16

Line 21 S-N Time: 14.43 - 14.57
 2545 127.2 start out crop of sill on rise to next level
 4645 232.2 end

Line 22 S-N Time: 15.04 - 15.45
 2670 133.45 on top of sill
 3977 188.8 middle of runway
 11342 567.05 start of 1.5 m rise
 13182 659.5 start of steep 2 m rise
 17929 896.4 start of steep rise >2 m
 19688 984.35 end, about 30 m from rise of basement.

Line 23 N-S Time: 16.00 - 16.35
 1129 64.5 steep descent
 6492 324.55 steep descent
 20375 1018.7 end

Line 24 S-N Time: 16.45 - 17.05
 0 0 start at trench 565911
 5442 272.05 end

04/08/16

Line 25 S-N Time: 12.20 - 13.21
 0 0 In nearby river section a sill was close to the surface
 4148 207.35 top of broad coastal near ridge
 5680 283.95 low wet part between ridges
 7748 385.85 close to river, top of ridge
 11989 559.4 change of direction, close to river
 13919 695.9 top of small ridge
 15974 798.65 top of small ridge
 16761 838 top of small ridge, start of gentle rise to the upper part
 19078 953.85 top of small stoney ridge with the 6 ponds, from here stones & blocks
 20865 1043.2 top level
 21145 1057.2 end

Line 26 N-S Time: 13.30 - 14.25
 793 39.6 edge of descent from highest level
 2085 104.2 top of stoney ridge with small ponds
 2804 140.15 top of small ridge
 4921 246 top of small ridge
 6718 335.85 top of small ridge

7344	367.15	stone pavement, angular oligomict stones
8737	436.8	top of small ridge, slight turn to the right to avoid wet area
12646	632.25	top of broad gravely ridge
19570	978.75	end

05/08/16

Line 27	S-N	Time: 10.45 - 11.15
0	0	Start close to coast, about 2 m of sediment on sill
6340	316.95	top of broad ridge close to small stream
7422	371.05	end of line at lake

Line 28	S-N	Time: 11.25 - 11.56
0	0	start on other side of lake
2698	134.85	top of small ridge
3289	164.3	carrying GPR 4 m over deeper water
6607	330.3	top of small ridge
8866	443.25	top of small ridge
9686	484.25	Ridge, with 6 ponds
10795	539.7	up on highest level
11776	588.75	end

Line 29	N-S	Time: 12.08 - 12.53
0	0	Start by trench
4358	217.85	small ridge
5323	266.1	small ridge
16341	817	carried GPR for 2 m over water
19552	977.55	end at coast

Line 30	S-N	Time: 13.56 - 15.05
1014	50.65	top of broad ridge
2533	126.6	carrying GPR over 2 m of water
5993	299.6	top of broad ridge
7818	390.85	close to lake
17252	862.55	indistinct ridge, in line with ponds
19221	961	end, perhaps on alluvial fan

Line 31	N-S	Time: 15.12 - 15.54
12349	617.4	top of broad ridge
78922	946.15	end on small ridge near coast

Line 32	S-N	Time: 16.05 - 16.45
6429	321.4	small ridge S of lakes
7581	379	change of direction to avoid water
8465	423.2	change of direction to get back on course
10723	536.1	small ridge N of lakes
12533	626.6	small ridge
17354	867.65	end, last 50 m perhaps alluvial fan

06/08/16		
Line 33	N-S	Time: 10.49 - 11.15
2324	116.15	small ridge
3867	193.3	very small ridge
5255	262.7	small ridge
6941	347	small ridge
87.02	435	end at small lake
Line 34	N-S	Time: 11.23 - 12.15
4853	242.6	small ridge
10323	516.1	start passing shallow stream
10774	538.65	end passing shallow stream
19749	987.4	end of line
Line 35	NW-SE	Time: 12.50 - 13.02
1188	59.35	start of blocky field
2692	134.55	end at lower lake
Line 36	S-N	Time: 13.05 - 13.14
470	23.45	start of blocky field
898	44.85	end of blocky field
1545	77.2	end of line at large lake
Line 37	N-S	Time: 13.16 - 13.22
1052	52.55	middle of small blocky field
1539	76.9	end at smaller lake
Line 38	NW-SE	Time: 13.26 - 13.35
2751	137.5	end
Line 39	NW-SE	Time: 13.42 - 13.50
3431	171.5	end
Line 40	N-S	Time: 13.55 - 14.00
2246	112.25	end
Line 41	N-S	Time: 14.07 - 14.11
2001	100	end
Line 42	N-S	Time: 14.20 - 14.23
838	41.85	end, very blocky
Line 43	S-N	Time: 14.25 - 14.29
993	49.6	End very blocky
Line 44	E-W	Time: 14.56 - 15.07

0	0	tie line. Start close to line 34
3463	173	crossing line 32
5215	260.7	end

Line 45	E-W	Time: 15.09 - 15.15
281	14	crossing line 31
2049	102.4	crossing line 30
2346	117.25	end

Line 46	E-W	Time: 15.17 - 15.20
0	0	tie line
369	18.4	crossing line 29
1519	75.9	crossing line 28
1765	88.2	end

Line 47	E-W	Time: 15.23 - 15.31
371	18.5	crossing line 27
2672	133.55	crossing line 26
3262	163.05	end line

07/08/16

Line 48	W-E	9.55 - 10.02
0	0	tie line
890	44.45	crossing line 25
2525	126.2	sample 567198, 25 m to the south
3335	166.7	end at stream

Line 49	E-W	10.11 - 10.30
0	0	tie line
6469	323.4	small stream

line 50	E-W	10.57 - 11.33
0	0	tie line
1605	80.2	getting more rich in boulders (close to alluvial fan)
18354	917.65	end at river

Line 51	S-N	12.28 - 12.45
195	9.7	sample point 567187, 20 m to the east
4147	207.3	dry river bed
4592	229.55	dry riverbed
7069	353.3	end of line at river cutting Lost pin to odometer wheel, taping it

Line 52	N-S	13.05 - 13.23
2636	131.75	sample 567182, 4 m to the east
2988	149.35	middle of dry riverbed
4766	238.25	sample point 567183

8119	405.9	end of line In southern part of line the basement should be close to the surface
<hr/>		
Line 53	E-W	15.30 - 15.50
9264	463.15	end of line at stream
<hr/>		
Line 54	W-E	16.02 - 16.30
1251	62.5	middle of small stream
6280	313.95	middle of stream
11728	586.35	sample point 5 m north of here
12241	612	end of line